Biophysical Fitness Landscape of the SARS-CoV-2 Delta Variant Receptor Binding Domain

Casey Patrick, Vaibhav Upadhyay, Alexandra Lucas and Krishna M. G. Mallela *

Department of Pharmaceutical Sciences, *Skaggs School of Pharmacy and Pharmaceutical Sciences, University of Colorado Anschutz Medical Campus, Aurora, CO, USA*

Correspondence to Krishna M.G. Mallela: *Department of Pharmaceutical Sciences, Skaggs School of Pharmacy and Pharmaceutical Sciences, University of Colorado Anschutz Medical Campus, 12850 E. Montview Blvd, MS C238-V20, Aurora, CO 80045, USA.* *krishna.mallela@cuanschutz.edu (K.M.G. Mallela)*
https://doi.org/10.1016/j.jmb.2022.167622
Edited by Eric O. Freed

Abstract

Among the five known SARS-CoV-2 variants of concern, Delta is the most virulent leading to severe symptoms and increased mortality among infected people. Our study seeks to examine how the biophysical parameters of the Delta variant correlate to the clinical observations. Receptor binding domain (RBD) is the first point of contact with the human host cells and is the immunodominant form of the spike protein. Delta variant RBD contains two novel mutations L452R and T478K. We examined the effect of single as well as the double mutations on RBD expression in human Expi293 cells, RBD stability using urea and thermal denaturation, and RBD binding to angiotensin converting enzyme 2 (ACE2) receptor and to neutralizing antibodies using isothermal titration calorimetry. Delta variant RBD showed significantly higher expression compared to the wild-type RBD, and the increased expression is due to L452R mutation. Despite their non-conservative nature, none of the mutations significantly affected RBD structure and stability. All mutants showed similar binding affinity to ACE2 and to Class 1 antibodies (CC12.1 and LY-CoV016) as that of the wild-type. Delta double mutant L452R/T478K showed no binding to Class 2 antibodies (P2B-2F6 and LY-CoV555) and a hundred-fold weaker binding to a Class 3 antibody (REGN10987), and the decreased antibody binding is determined by the L452R mutation. These results indicate that the immune escape from neutralizing antibodies, rather than increased receptor binding, is the main biophysical parameter that determined the fitness landscape of the Delta variant RBD.

Introduction

In late 2019, a novel coronavirus (2019-nCoV), later renamed as severe acute respiratory syndrome coronavirus 2 (SARS-CoV-2), was discovered in Wuhan, China and quickly became the center of the ongoing pandemic coronavirus disease 19 (COVID-19). SARS-CoV-2 enters human host cells with its spike protein interacting with the angiotensin converting enzyme 2 (ACE2) located on the cell surface.[1–5] A specific structural region within the spike protein, known as the receptor binding domain (RBD), binds to the ACE2 receptor. SARS-CoV-2 has been shown to continuously mutate in multiple regions of the spike protein leading to new variants of interest (VOI) and more severe variants of concern (VOC). VOCs in general have been shown to have increased infectivity,[6–9] enhanced ACE2 binding,[10–12] escape from the human immune system,[4,10,13] and evade FDA-approved monoclonal antibody therapies.[4,6,9] To date, there have been five known VOCs, which include Alpha, Beta, Gamma, Delta, and the Omicron.

Out of all the five VOCs, Omicron is the most transmissible variant, whereas Delta is the most virulent leading to more severe symptoms and an increased mortality among infected patients. Delta variant arose from the B.1.617 lineage, and is specifically labeled as variant B.1.617.2. It was first identified in India and has since been accounted for the majority of COVID-19 deaths worldwide.[14,15] Delta variant has been shown to have higher viral titers in COVID-19 patients compared to previous variants.[15–17] Prior to the emergence of Omicron variant, increased breakthrough infections of COVID-19 in vaccinated patients have been attributed to the Delta variant.[16–19] A single dose of vaccination was found to be only 33% effective in protecting against the Delta variant as opposed to 48.7% against the Alpha variant, and two vaccination doses were only 88% effective for the Delta variant compared to 93.7% for the Alpha variant.[20]

Delta variant introduces several mutations in the N-terminal domain (NTD), RBD, and the furin cleavage site of the spike protein that makes it distinct from the unmutated, wild-type (WT) virus.[21] Unlike previous variants, which have had mutations that have been predicted by *in vitro* evolution through biophysical parameters such as ACE2 binding, the mutations in the Delta variant, particularly in the RBD, have not previously been predicted to lead to a more dangerous variant.[12,22] Delta RBD contains two mutations which change the characteristic nature of the amino acid: a hydrophobic amino acid leucine mutated to a positively charged amino acid arginine at position 452 (L452R) and an uncharged amino acid threonine mutated to a positively charged lysine at position 478 (T478K) in the primary structure of the protein.[6,9,14,23,24] None of these two mutations are part of the RBDs of previously discovered VOCs that include Alpha (N501Y), Beta (K417N/E484K/N501Y), or Gamma (K417T/E484K/N501Y). The newly discovered Omicron VOC RBD contains only the T478K mutation and not the L452R mutation.[25]

Analyzing the biophysical parameters that determine the fitness landscape of viruses is of considerable interest in recent years, particularly in the case of HIV, influenza, dengue, hepatitis C, and other retroviruses.[26–31] In the case of SARS-CoV-2 RBD, we along with others have recently shown that increased receptor binding, escape from neutralizing antibodies, and maintaining protein structure, stability, and expression despite the non-conservative nature of amino acid mutations are important parameters that direct the natural selection of mutations and determine the biophysical fitness landscape of emerging variants.[10,32–37] These biophysical analyses were done on Alpha, Beta, and Gamma VOCs before the Delta variant has emerged. Whether the two novel mutations of the Delta RBD, which were not part of the previous VOCs, follow similar natural selection principles is not clear. This study examined the effect of the two single amino acid mutations L452R, T478K and the double mutant L452R/T478K on the biophysical properties (structure, stability, receptor binding, and binding to neutralizing antibodies) of the RBD. Our results indicate that the Delta RBD does not show increased ACE2 receptor binding compared to the WT RBD unlike the previous VOCs (Alpha, Beta, and Gamma), but shows increased protein expression, consistent with increased spike protein expression and viral titers in Delta patients, and escapes multiple neutralizing antibodies. Increased expression and antibody escape is determined by the L452R mutation.

Results

L452R mutation enhances Delta variant RBD expression

VOCs including Delta are known to have decreased levels of neutralization titers in both vaccinated and unvaccinated individuals.[15–17,38] In addition, Delta variant COVID-19 patients have viral titers ten times higher than that of the other variants.[15] A plausible explanation is that the mutations in the Delta variant might have a selective advantage in terms of increased expression of viral proteins over the wild-type virus. Higher quantities of the viral proteins could allow for more virus particles to be created.[39] In order to test if this clinical observation could be correlated with the increased expression of RBD, which is a major part of the spike protein, expression of the wild-type (WT) RBD and its Delta mutants (L452R, T478K, and L452R/T478K) was tested in human embryonic kidney cells (Expi293 HEK). HEK cells can be used to test the mutation effects on protein expression levels, since protein expression profiles and the quality control mechanisms in different human cells are similar. In addition, SARS-CoV-2 has been shown to infect the kidney cells,[40–42] and HEK cells naturally express the ACE2 receptor. After 48 hours of transfection, secreted proteins in the supernatants were analyzed using SDS-PAGE (Figure 1(A)) and the expression levels were quantified as a ratio of the mutant over WT RBD (Figure 1(B)). Both the L452R single mutant and the Delta double mutant L452R/T478K showed ∼70% higher expression compared to WT RBD (Figure 1(B)). No significant differences in expression were observed for the T478K mutant compared to the WT RBD. These results indicate that the L452R mutation is responsible for the increased expression of Delta variant RBD and possibly the spike protein expression.

None of the Delta mutations significantly affect global protein structure

Both mutations L452R and T478K are non-conservative mutations where one type of amino
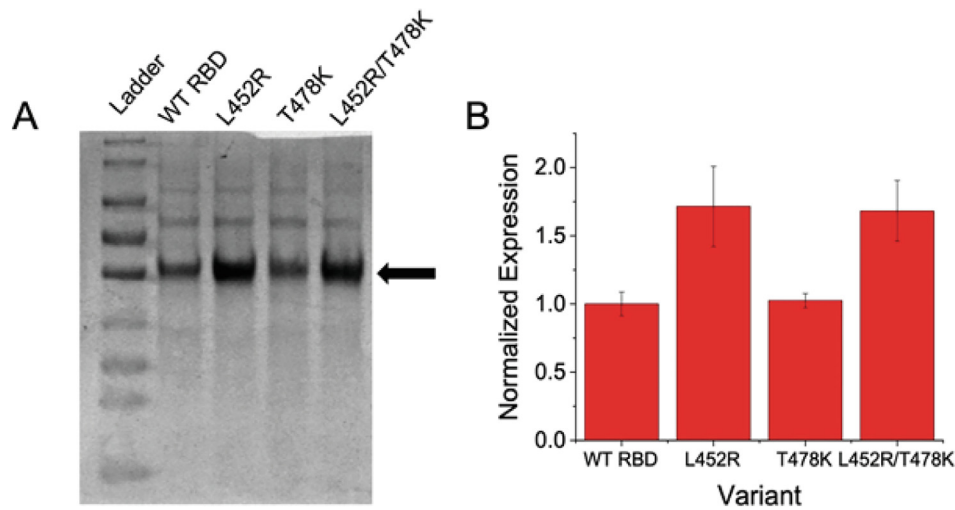
Figure 1. Expression differences between WT RBD and its Delta mutants. (A) SDS-PAGE showing relative expression of RBD variants 48 hours after transfection. Ladder represents the molecular markers (from top to bottom: 180, 130, 100, 70, 55, 40, 35, 25, and 15 kDa, respectively). (B) Normalized relative expression of RBD variants. Results in panel A were repeated in triplicate to obtain the data shown in panel B.

acid is mutated to another type of amino acid with differing physical properties. Such mutations tend to destabilize proteins if the amino acid prior to mutation is involved in stabilizing the protein structure. To test the effect of mutations on RBD structure, we used far-UV circular dichroism and fluorescence spectroscopy. Figure 2(A) shows SDS-PAGE of purified proteins, and the single bands on the gel show the high purity of protein samples used for biophysical analyses reported in this manuscript. Figure 2(B) shows the far-UV circular dichroism (CD) and Figure 2(C) shows the intrinsic protein fluorescence spectra of the WT RBD and its Delta single mutants and the double mutant. Spectra of the WT match those reported in the literature.[10,43–45] More importantly, none of the mutations caused significant changes in the spectra, implying that the Delta mutations do not significantly affect the global protein structure.

None of the Delta mutations enhance RBD stability

Protein stability could provide valuable insight into both the viability and flexibility of proteins and has been shown to play a big role in the fitness of viruses.[27,46] To evaluate how the Delta mutations alter the RBD stability, both thermal and urea denaturation melts were utilized. Change in protein structure with increase in temperature (Figure S1) was fit
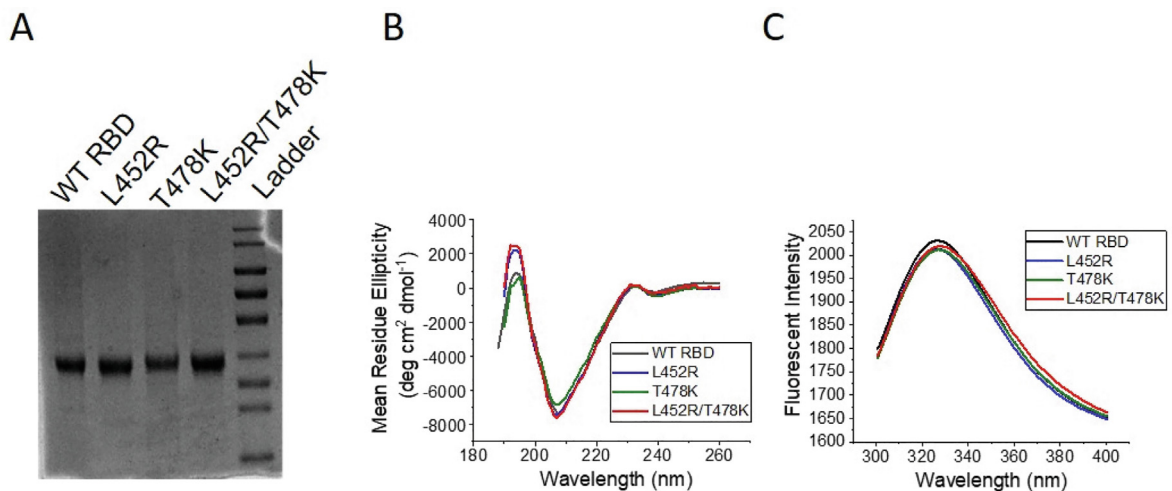

Figure 2. (A) SDS-PAGE of purified RBD constructs. Ladder represents the molecular markers (from top to bottom: 180, 130, 100, 70, 55, 40, 35, 25, and 15 kDa, respectively). (B) Far-UV circular dichroism spectra of WT RBD and its Delta mutants. (C) Intrinsic fluorescence spectra of WT RBD and its Delta mutants.

to a two-state unfolding model (Eq. (1) in Materials and Methods) to obtain the midpoint melting temperature (T_m) of the proteins. Since the thermal melts are not reversible, T_m values can only be used as a qualitative measure of protein stability.[10,47] Table S2 lists the mean fit parameters obtained from three independent batches of protein expression. Compared to WT RBD, which showed a T_m of 56.1 ± 0.7 °C, L452R displayed a similar stability of 56.5 ± 0.2 °C, while T478K displayed a slightly decreased T_m of 54.1 ± 0.1 °C. However, the Delta double mutant L452R/T478K exhibited a T_m of 56.6 ± 0.2 °C, similar to that of the WT (Figure S1 and Table S1).

Urea denaturation melts of RBD variants are completely reversible (Figure S2). The native signal showed a large change with denaturant concentration, which might indicate partial unfolding and non-2-state unfolding behavior that needs to be further probed. However, since we observed only a single sigmoidal transition, denaturant melts were fit to a 2-state unfolding model (Eq. (2) in Materials and Methods) to obtain Gibbs free energy of unfolding in the absence of denaturant ($\Delta G°_{unf}$) and the slope of linear variation of ΔG_{unf} with urea concentration (m-value) for each variant. Table S2 lists the mean fit parameters obtained from three independent batches of protein expression. WT RBD showed a $\Delta G°_{unf}$ of 8.1 ± 0.3 kcal/mol with a m-value of −1.24 ± 0.06 kcal/mol/M [urea]. Both single mutants L452R and T478K showed similar stability as that of the WT RBD. L452R displayed a $\Delta G°_{unf}$ of 8.1 ± 0.2 kcal/mol with a m-value of −1.43 ± 0.04 kcal/mol/M [urea], while T478K showed $\Delta G°_{unf}$ and m-values of 7.9 ± 0.5 kcal/mol and −1.37 ± 0.09 kcal/mol/M [urea], respectively. Delta double mutant L452R/T478K was also found to have similar stability as that of the WT RBD, with a $\Delta G°_{unf}$ of 8.6 ± 0.3 kcal/mol and an m-value of −1.53 ± 0.06 kcal/mol/M [urea] (Table S2). These equilibrium stability values obtained from urea denaturant melts agree quite well with the trends observed with thermal denaturation melts (Table S1) and indicate that none of the Delta mutants significantly affect RBD stability.

Delta mutations do not show increased affinity for ACE2 receptor

Since SARS-CoV-2 enters host cells with its RBD binding to ACE2, the relative binding affinity of the RBD can play a key role in how variants are evolving. An increase in the affinity of the Delta variant to ACE2 could allude to a potential mechanism where the VOC allows more viral entry into host cells. Previous VOCs (Alpha, Beta, and Gamma) have shown enhanced ACE2 binding compared to the WT RBD.[10] Location of the two amino acid mutations L452R and T478K in the Delta variant RBD with respect to ACE2 binding interface is shown in Figure 3(A). None of the

two mutations are part of the ACE2 interface. Figure 4 shows isothermal titration calorimetry (ITC) thermograms for the WT RBD and Delta mutants, and Table 1 lists the average fit parameters from three independent batches of protein expression. WT RBD binding to ACE2 shows a typical exothermic reaction with a K_d of 10.0 ± 3.1 nM and a ΔH value of −11.8 ± 0.2 kcal/mol. None of the Delta mutations significantly altered the binding affinity of RBD for ACE2. Both L452R and T478K mutants and the Delta double mutant L452R/T478K displayed similar K_d values of 6.2 ± 3.7 nM, 17.1 ± 4.8 nM, and 10.8 ± 3.3 nM, respectively, similar to that of the WT RBD (Table 1).

Delta RBD mutations do not escape Class 1 antibodies

Clinical observations associated with Delta variant could be related to SARS-CoV-2 escaping the human immune system. Neutralizing antibodies against SARS-CoV-2 RBD have been found to belong to four major classes depending on the mechanism of action and the location of their epitopes on the RBD.[48,49] SARS-CoV-2 spike protein is a trimer in its native state and exists in multiple conformations, mainly RBD in "up" position that is accessible for binding to ACE2 or in "down" position in which RBD is buried and not accessible for ACE2 binding.[50–52] Class 1 antibodies bind to RBD in the up conformation and compete with ACE2 binding. Class 2 antibodies bind to RBD both in the up or down conformations, and their epitope partially overlaps with the ACE2 binding site and hence compete against ACE2 binding. Class 3 antibodies bind to RBD in both up or down positions with their epitope on RBD far away from ACE2 binding site, and hence can neutralize the RBD through an uncompetitive mechanism. Class 4 antibodies are relatively rare as their epitope is close to the hinge region connecting RBD to the rest of the spike protein, which is relatively buried compared to other epitopes, and none of the VOCs contain mutations in this region. Since the first step in neutralization is binding of antibodies to RBD, we examined how the Delta mutations affect RBD binding to the three major classes of antibodies.

One of the first Class 1 antibodies that was identified from patients recovered from WT SARS-CoV-2 infection was CC12.1.[53] Location of the two Delta mutants L452 and T478 in RBD with respect to the CC12.1 binding interface is shown in Figure 3 (B). Binding of WT RBD and its Delta mutants to CC12.1 single chain variable fragment (ScFv) was measured using ITC (Figure 5), and the average thermodynamic parameters obtained from fitting the data from three independent batches of protein expression was included in Table 2. All proteins showed similar exothermic binding profiles. WT RBD binds to CC12.1 with a K_d of 23.9 ± 5.7 nM. Both Delta single mutants L452R and T478K as well as the double mutant L452R/T478K either bind with
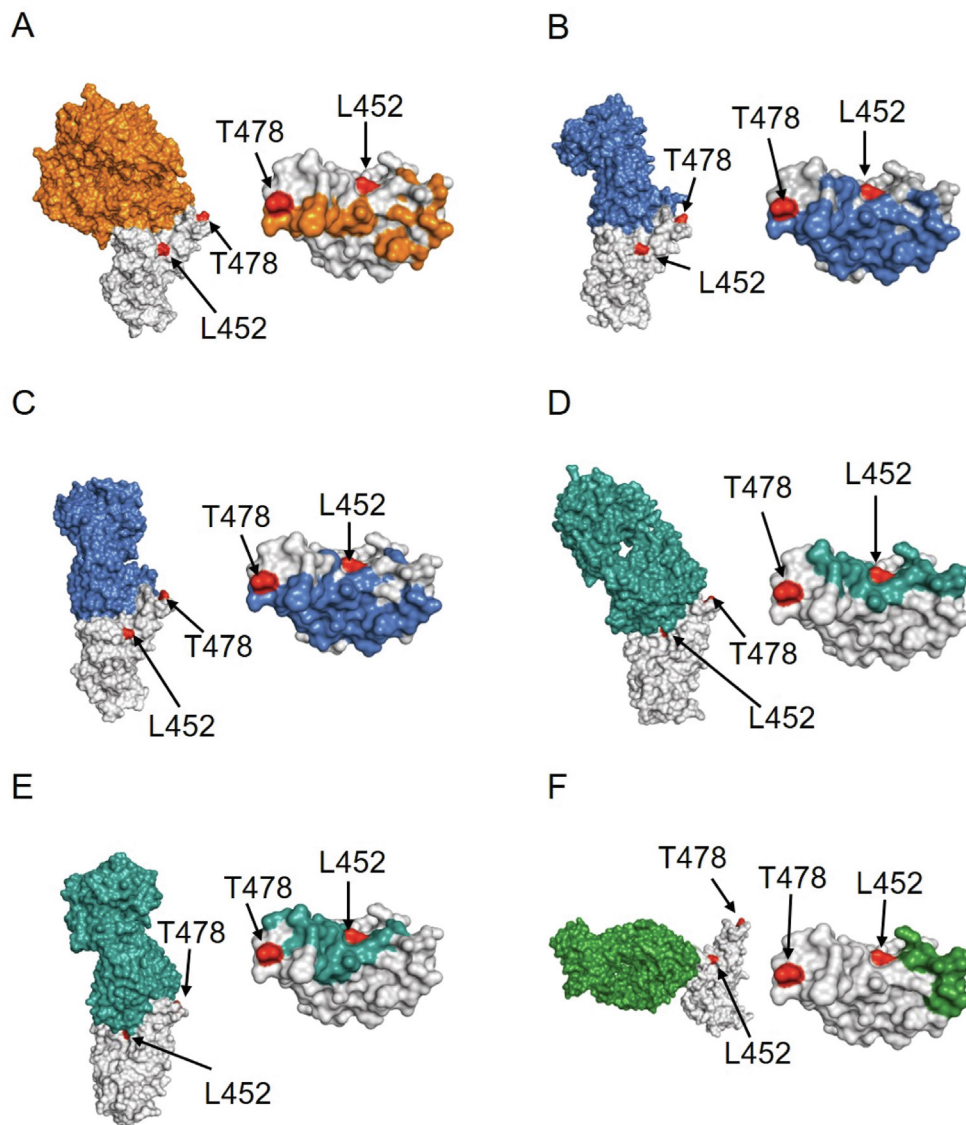
Figure 3. Structural analysis of the location of Delta mutants L452 and T478 (red colored) with respect to RBD (gray colored) complexes with (A) ACE2 receptor (orange colored; PDB ID 6moj), (B) Class 1 antibody CC12.1 (blue colored; PDB ID 6xc2), (C) FDA-approved Class I therapeutic antibody LY-CoV016 (blue colored; PDB ID 7c01), (D) Class 2 antibody P2B-2F6 (teal colored; PDB ID: 7bwj), (E) FDA-approved Class 2 antibody LY-CoV555 (teal colored; PDB ID: 7kmg) and (F) FDA-approved Class 3 antibody REGN10987 (green colored; PDB ID 6xdg). Left panels show the complex structures and right panels show the location of the interacting residues in RBD with respect to the binding interfaces.

a similar affinity (similar K_d value for T478K) or with a higher affinity (lower K_d values for L452R and L452R/T478K), implying that the Delta variant RBD does not escape from Class 1 antibodies. ITC binding data is also consistent with the location of these two residues L452 and T478 with respect to the epitope of CC12.1 on RBD (Figure 3(B)). The two mutations in the Delta variant RBD are located far from the CC12.1 epitope, and do not affect the interactions between RBD and CC12.1.[54,55]

As of January 2022, FDA approved four therapeutic antibodies for emergency use authorization (EUA): Eli Lilly's LY-CoV016 (Etesevimab) and LY-CoV555 (Bamlanivimab), and Regeneron's REGN10933 (Casirivimab) and REGN10987 (Imdevimab). LY-CoV016 and REGN10933 are Class 1 antibodies whose epitopes are very similar on RBD.[56,57] LY-CoV555 is a Class 2 antibody, whereas REGN10987 is a Class 3 antibody. To determine whether Delta variant escapes FDA-approved Class 1 antibodies, we tested WT RBD and its Delta mutants binding to LY-CoV016 in ScFv format. Figure 3(C) shows the location of the two residues L452 and T478 with respect to the RBD interface with LY-CoV016. Figure 6 shows the ITC binding data for the single
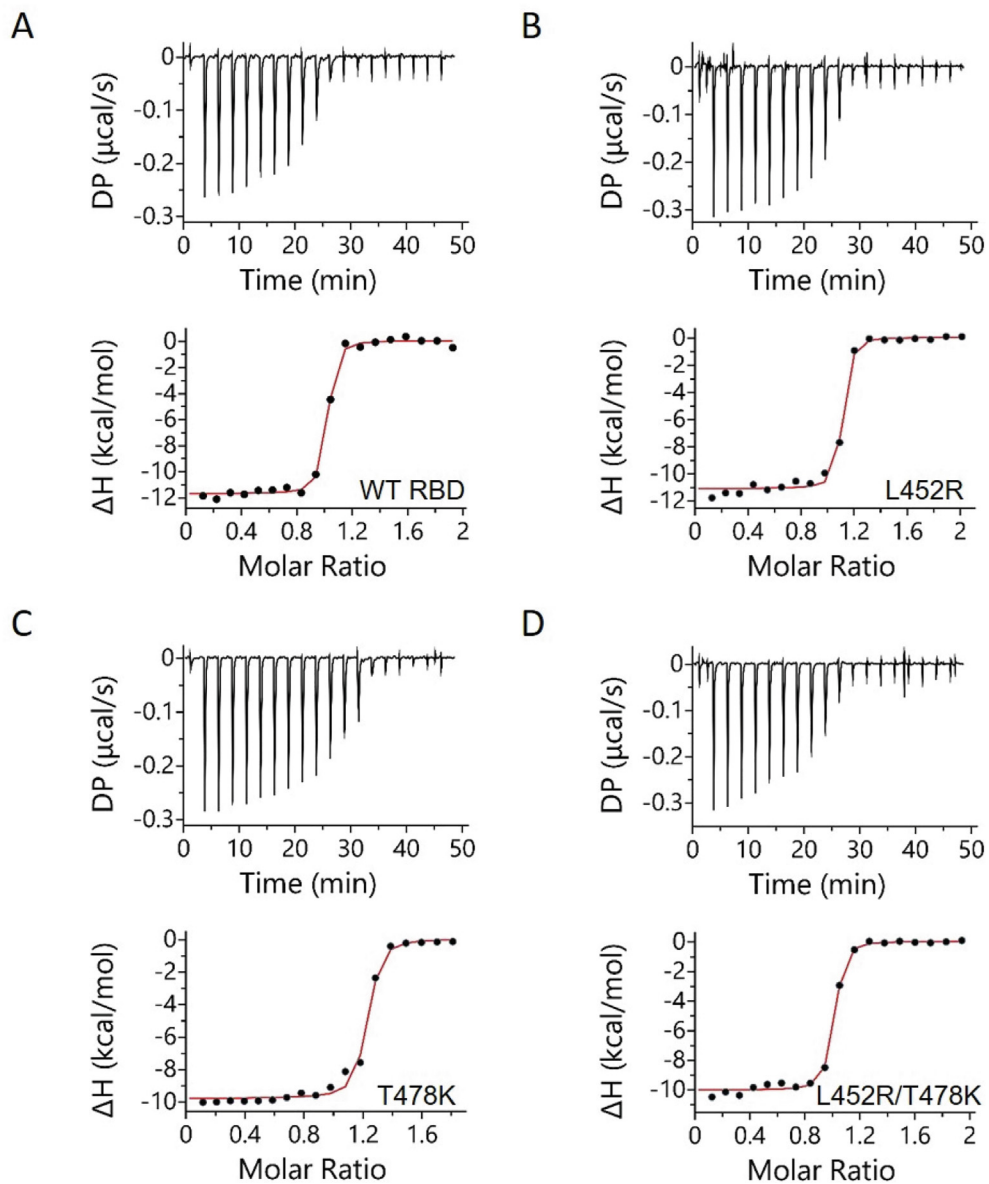
Figure 4. ITC analysis of WT RBD and its Delta mutants binding to ACE2. Top panels represent the raw differential power vs. time thermographs, while bottom panels represent the integrated heat plots.

Table 1 Thermodynamic parameters of WT RBD and its Delta mutants binding to ACE2 receptor.

RBD Variant	K_d (nM)	N	ΔH (kcal/mol)	ΔG (kcal/mol)	−TΔS (kcal/mol)
WT	10.0 ± 3.1	1.0 ± 0.0	−11.8 ± 0.2	−10.7 ± 0.2	1.0 ± 0.3
L452R	6.2 ± 3.7	1.0 ± 0.0	−11.3 ± 0.2	−11.1 ± 0.3	0.3 ± 0.4
T478K	17.1 ± 4.8	1.0 ± 0.1	−10.0 ± 0.2	−10.4 ± 0.2	− 0.4 ± 0.3
L452R/T478K	10.8 ± 3.3	0.9 ± 0.0	−10.1 ± 0.2	−10.7 ± 0.2	− 0.6 ± 0.3

and double mutants. All interactions displayed exothermic binding profiles. Table 3 lists the average parameters obtained from fitting the ITC data from three independent batches of protein expression to a one-site binding model. WT RBD binds

to LY-CoV016 with a K_d of 49.3 ± 10.1 nM. Both single mutants L452R and T478K and the double mutant L452R/T478K bind to LY-CoV016 with a stronger affinity, implying that none of the Delta mutations escape LY-CoV016. This is consistent
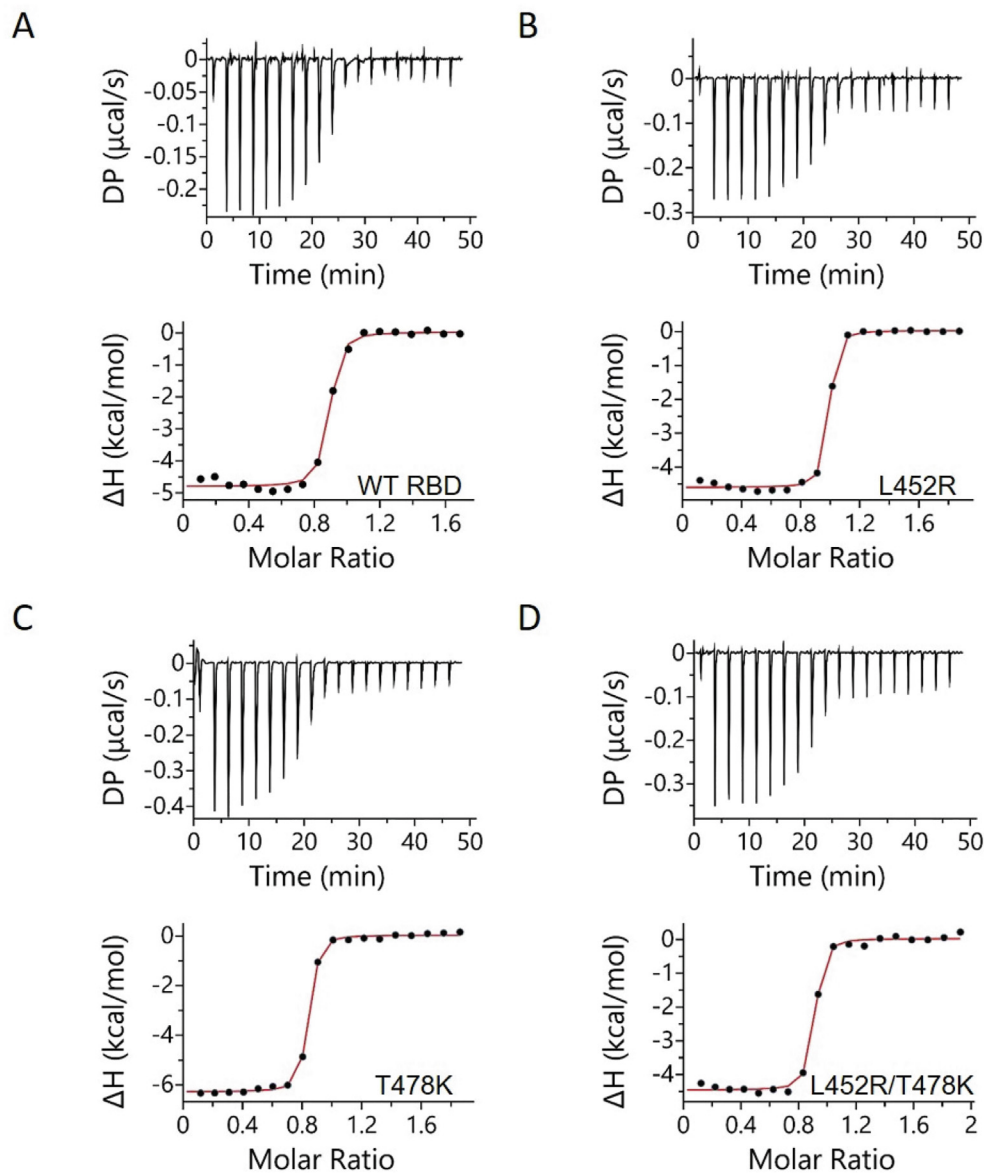
Figure 5. ITC analysis of WT RBD and its Delta mutants binding to Class 1 antibody CC12.1 ScFv. Top panels represent the raw differential power vs. time thermographs, while bottom panels represent the integrated heat plots.

Table 2 Thermodynamic parameters of WT RBD and its Delta mutants binding to Class 1 antibody CC12.1 ScFv.

RBD Variant	K_d (nM)	N	ΔH (kcal/mol)	ΔG (kcal/mol)	−TΔS (kcal/mol)
WT	23.9 ± 5.7	0.9 ± 0.1	−5.2 ± 0.5	−10.2 ± 0.1	−5.1 ± 0.4
L452R	13.0 ± 3.4	0.9 ± 0.0	−4.6 ± 0.1	−10.6 ± 0.2	−5.9 ± 0.2
T478K	23.1 ± 2.3	0.8 ± 0.1	−6.2 ± 0.1	−10.3 ± 0.1	−4.1 ± 0.1
L452R/T478K	12.4 ± 7.3	0.9 ± 0.0	−4.7 ± 0.2	−10.6 ± 0.3	−6.0 ± 0.4

with the location of the two residues L452 and T478 with respect to the RBD binding interface with LY-CoV016 (Figure 3(C)), and also consistent with binding of Delta mutants to another Class 1 anti-body CC12.1 described above (Figure 5 and Table 2).

L452R mutation determines Delta variant escape from Class 2 antibodies

While the Delta variant does not evade Class 1 antibodies, a large amount of clinical data suggests that neutralizing antibodies discovered
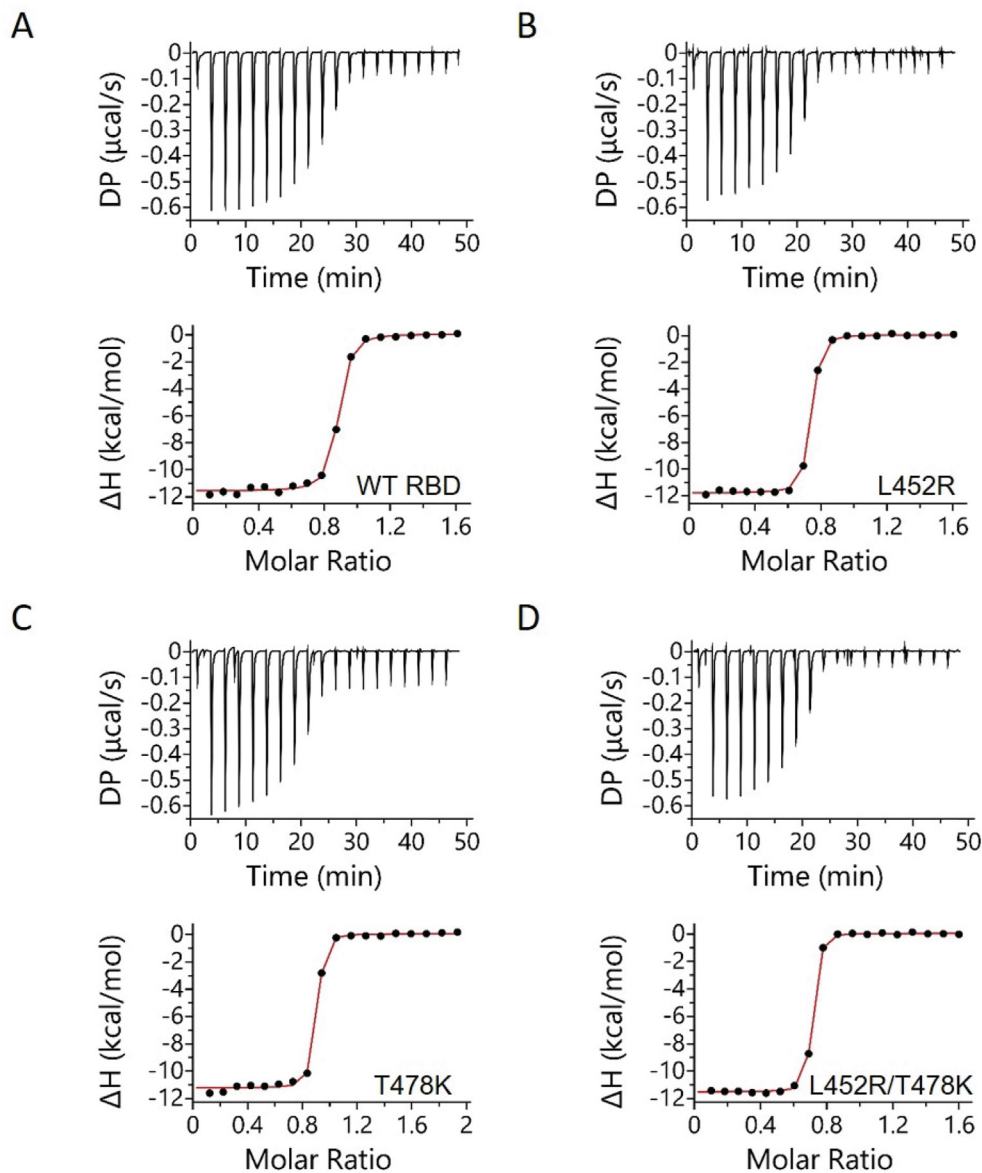
Figure 6. ITC analysis of WT RBD and its Delta mutants binding to FDA-approved Class 1 therapeutic antibody LY-CoV016 ScFv. Top panels represent the raw differential power vs. time thermographs, while bottom panels represent the integrated heat plots.

Table 3 Thermodynamic parameters of WT RBD and its Delta mutants binding to FDA-approved Class 1 therapeutic antibody LY-CoV016 ScFv.

RBD Variant	K_d (nM)	N	ΔH (kcal/mol)	ΔG (kcal/mol)	$-T\Delta S$ (kcal/mol)
WT	49.3 ± 10.1	0.9 ± 0.0	−11.7 ± 0.1	−9.8 ± 0.1	1.9 ± 0.2
L452R	23.4 ± 2.8	0.8 ± 0.1	−11.9 ± 0.1	−10.2 ± 0.1	1.7 ± 0.1
T478K	15.4 ± 3.0	0.8 ± 0.1	−11.4 ± 0.1	−10.5 ± 0.1	0.9 ± 0.2
L452R/T478K	10.8 ± 1.4	0.8 ± 0.1	−12.0 ± 0.4	−10.7 ± 0.1	1.3 ± 0.4

against WT SARS-CoV-2 are not effective in neutralizing emerging VOCs.[58] Similar to CC12.1, P2B-2F6 is one of the first neutralizing antibodies discovered in recovered COVID-19 patients.[59,60]

P2B-2F6 is a Class 2 antibody.[48,49] We examined whether Delta variant escapes from Class 2 antibodies by determining the binding of WT RBD and its Delta mutants to P2B-2F6 ScFv. Location of
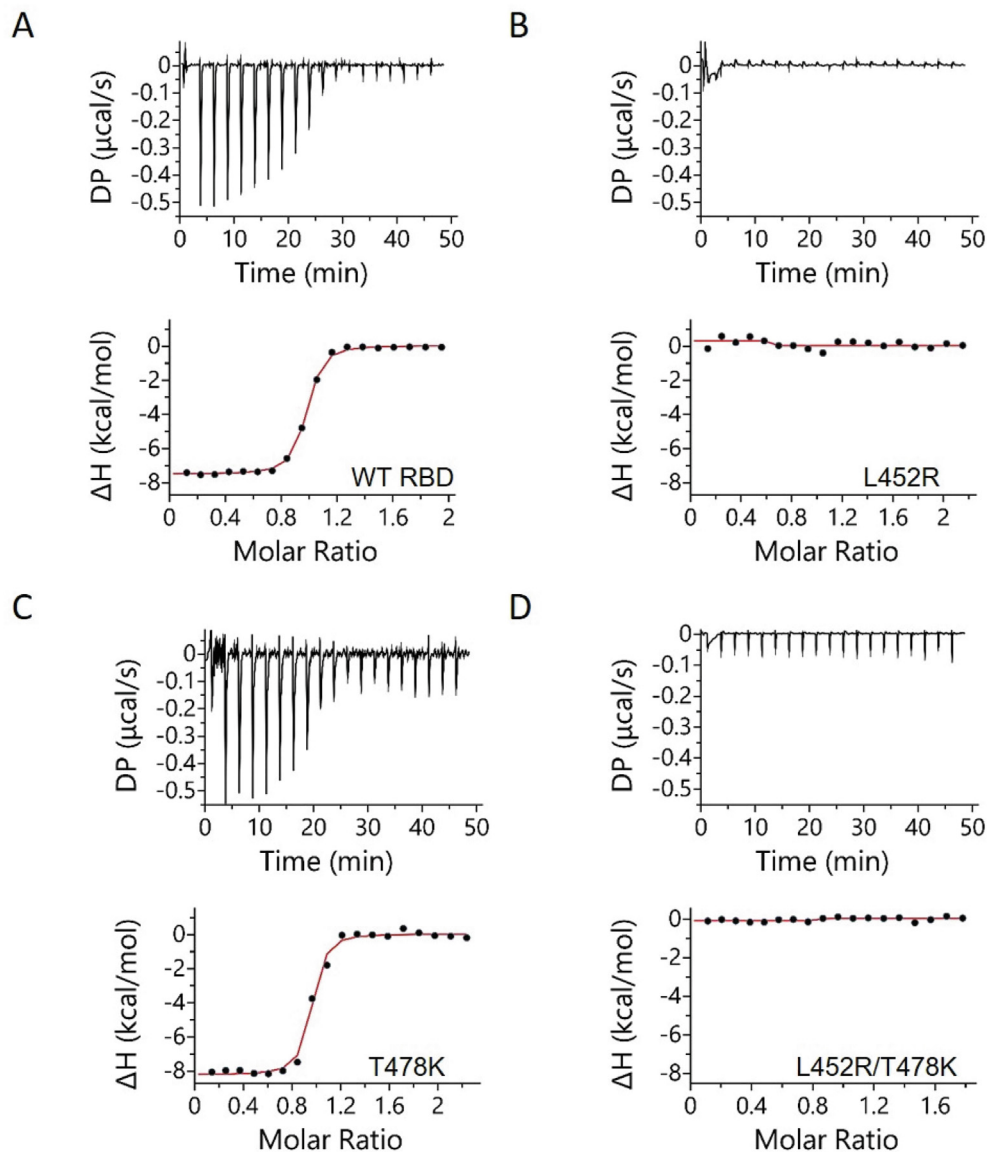
Figure 7. ITC analysis of WT RBD and its Delta mutants binding Class 2 antibody P2B-2F6 ScFv. Top panels represent the raw differential power vs. time thermographs, while bottom panels represent the integrated heat plots.

the two residues L452 and T478 in RBD with respect to its binding interface with P2B-2F6 is shown in Figure 3(D). Figure 7 shows the ITC binding curves and Table 4 lists the thermodynamic parameters obtained from fitting ITC data from three independent batches of protein expression to a one-site binding model. Both WT RBD and T478K show similar K_d values of 81.4 ± 6.2 nM and 80.5 ± 6.3 nM, respectively. However, L452R resulted in a complete loss of binding (Figure 7). Similar results were observed for the Delta double mutant L452R/T478K. These results indicate that the Delta variant escapes Class 2 antibodies, and the escape is determined by the L452R mutation. Our results on the effect of L452R mutation on RBD binding to P2B-2F6 are also consistent with a deep mutational scanning analysis that indicates

L452R as one of the possible immune-escaping hotspots.[61]

We further examined whether Delta variant escapes FDA-approved Class 2 antibody LY-CoV555.[62,63] Location of the two residues L452 and T478 in RBD with respect to its interface with LY-CoV555 is shown in Figure 3(E). Figure 8 shows the ITC binding curves for WT RBD and its Delta mutants, and Table 5 lists the mean thermodynamic parameters obtained from fitting ITC data from three independent batches of protein expression to one-site binding model. WT RBD binds to LY-CoV555 ScFv with a K_d of 3.8 ± 1.9 nM. T478K mutant shows a similar binding affinity to LY-CoV555 with a K_d of 9.0 ± 4.6 nM. This was however not the case for the L452R mutation and the Delta double mutant L452R/T478K. Both showed

Table 4 Thermodynamic parameters of WT RBD and its Delta mutants binding to Class 2 antibody P2B-2F6 ScFv.

RBD Variant	K_d (nM)	N	ΔH (kcal/mol)	ΔG (kcal/mol)	−TΔS (kcal/mol)
WT	81.4 ± 6.2	0.9 ± 0.0	−8.0 ± 0.5	−9.5 ± 0.1	−1.5 ± 0.5
L452R	No binding	–	–	–	–
T478K	80.5 ± 6.3	0.9 ± 0.0	−8.7 ± 0.4	−9.5 ± 0.0	−0.8 ± 0.4
L452R/T478K	No binding	–	–	–	–

Figure 8. ITC analysis of WT RBD and its Delta mutants binding to FDA-approved Class 2 therapeutic antibody LY-CoV555 ScFv. Top panels represent the raw differential power vs. time thermographs, while bottom panels represent the integrated heat plots.

no binding to LY-CoV555 (Figure 8). These results indicate that Delta variant escapes Class 2 antibodies, and the escape is determined by the L452R mutation, which is consistent with escape from another Class 2 antibody P2B-2F6 described above (Figure 7 and Table 4).

L452R mutation determines Delta variant escape from Class 3 antibodies

We also examined whether Delta variant escapes Class 3 antibodies. FDA-approved antibody therapeutics contain a Class 3 antibody

REGN10987. Location of the two residues L452 and T478 in RBD with respect to its interface with REGN10987 is shown in Figure 3(F). Figure 9 shows the ITC binding curves of WT RBD and its Delta mutants, and Table 6 lists the mean thermodynamic parameters obtained from fitting ITC data from three independent batches of protein expression to a one-site binding model. Both WT RBD and T478K mutant showed similar binding affinity with K_d values of 34.3 ± 8.1 nM and 15.9 ± 1.9 nM, respectively. This was not the case for both the L452R mutant and the Delta double mutant L452R/T478K. Both proteins showed a ~100 fold weaker binding affinity with K_d values of 1,340 ± 100 nM for the L452R mutant and 1,150 ± 100 nM for the Delta double mutant

(Table 6). These results indicate that the Delta variant escapes Class 3 antibodies, and the escape is determined by the L452R mutation.

Discussion

SARS-CoV-2 Delta variant has adapted unlike any other previous VOCs (Alpha, Beta, and Gamma). It is the VOC which is responsible for more severe symptoms and the maximum mortality among infected patients compared to other VOCs including Omicron. Deep mutational scanning has been able to predict that the previous VOCs had a high probability of becoming dominant strains, yet these studies were unable to predict the two novel mutations in the Delta
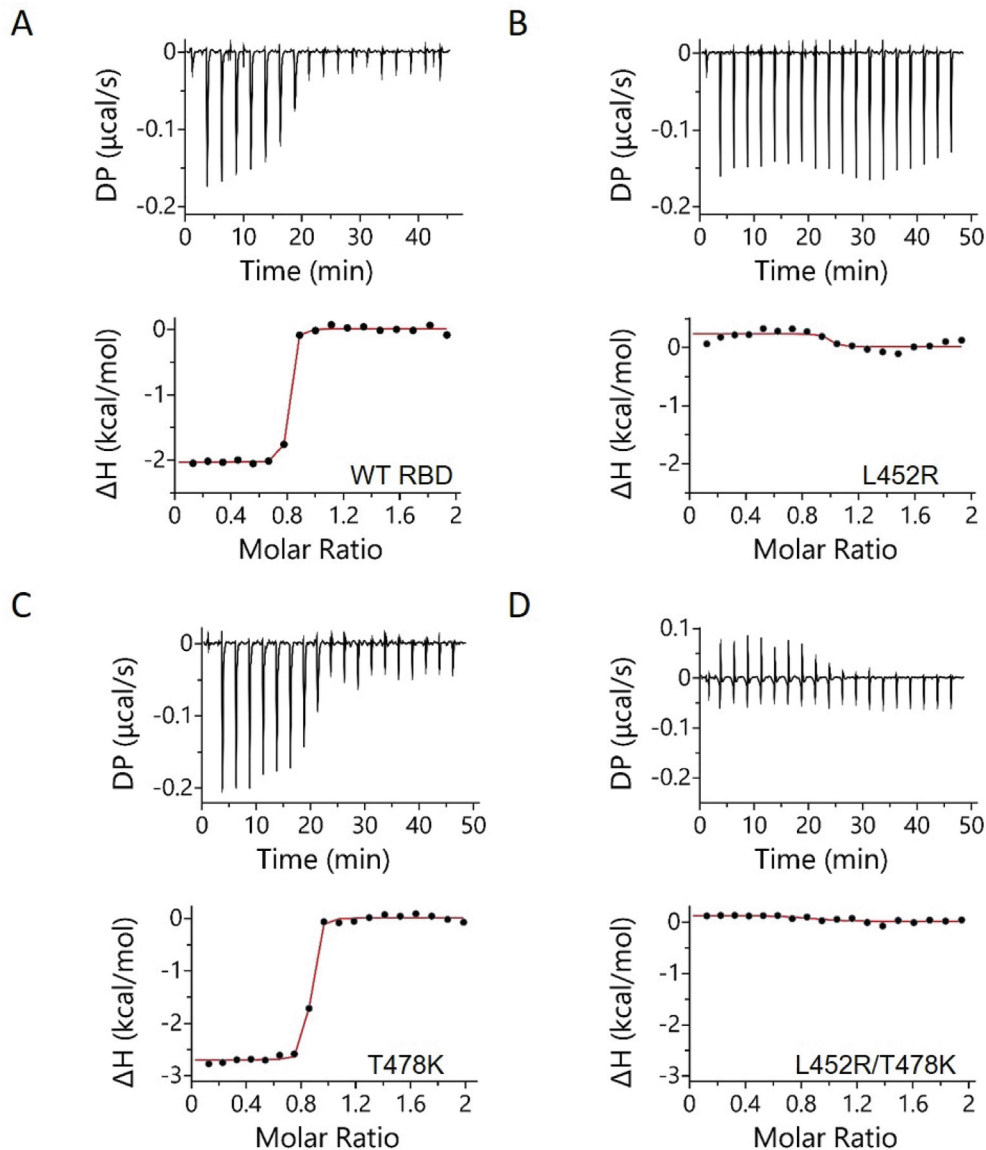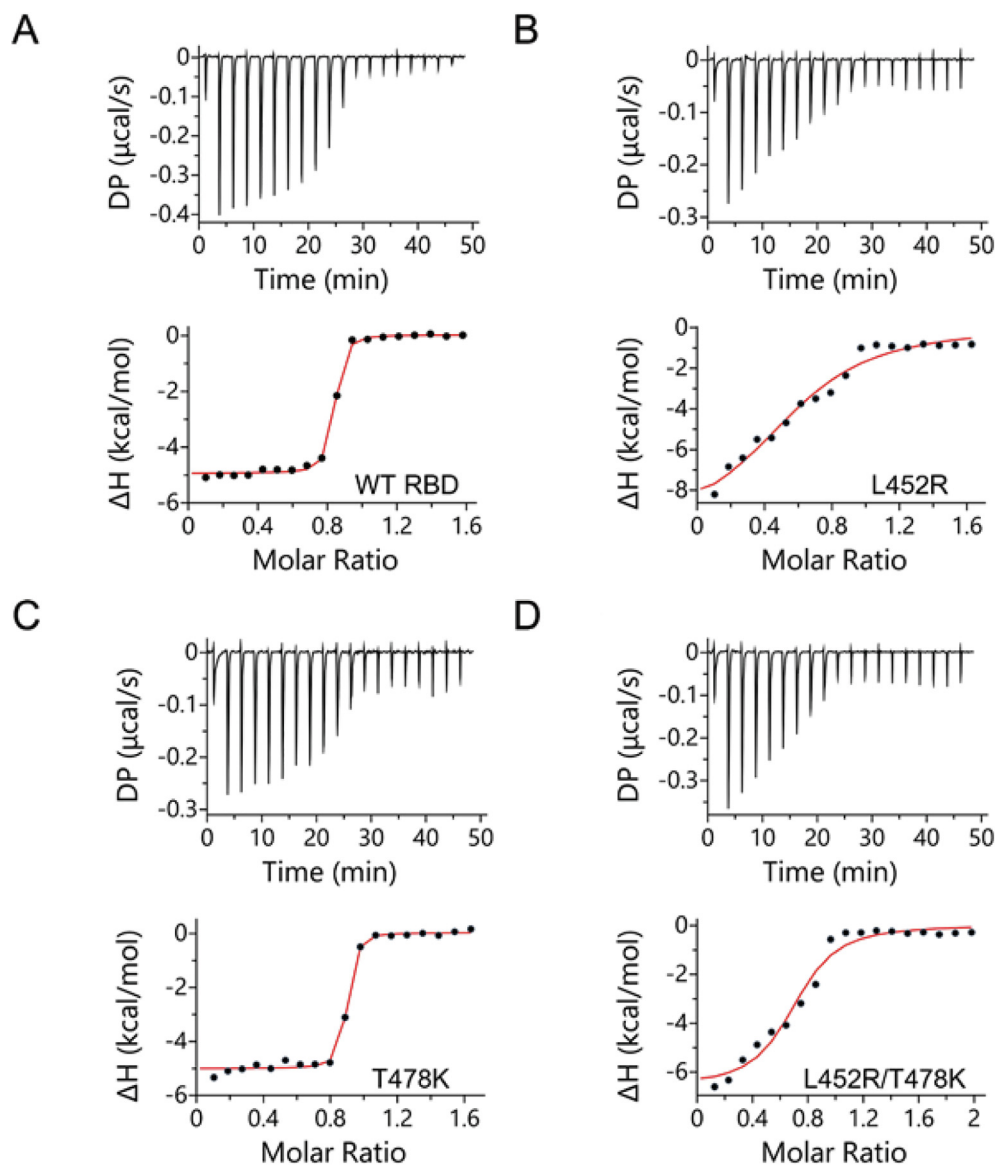

Figure 9. ITC analysis of WT RBD variant and its Delta mutants binding to FDA-approved Class 3 therapeutic antibody REGN987 ScFv. Top panels represent the raw differential power vs. time thermographs, while bottom panels represent the integrated heat plots.

Table 5 Thermodynamic parameters of WT RBD and its Delta mutants binding to FDA-approved Class 2 therapeutic antibody LY-CoV555 ScFv.

RBD Variant	K_d (nM)	N	ΔH (kcal/mol)	ΔG (kcal/mol)	$-T\Delta S$ (kcal/mol)
WT	3.8 ± 1.9	0.8 ± 0.1	−2.0 ± 0.1	−11.3 ± 0.3	−9.3 ± 0.3
L452R	No binding	–	–	–	–
T478K	9.0 ± 4.6	0.8 ± 0.0	−2.7 ± 0.1	−10.8 ± 0.3	−8.1 ± 0.3
L452R/T478K	No binding	–	–	–	–

Table 6 Thermodynamic parameters of WT RBD and its Delta mutants binding to FDA-approved Class 3 therapeutic antibody REGN10987 ScFv.

RBD Variant	K_d (nM)	N	ΔH (kcal/mol)	ΔG (kcal/mol)	$-T\Delta S$ (kcal/mol)
WT	34.3 ± 8.1	0.8 ± 0.1	−5.0 ± 0.1	−10.0 ± 0.1	−5.1 ± 0.2
L452R	1,340 ± 100	0.8 ± 0.1	−8.7 ± 1.3	−7.6 ± 0.3	1.1 ± 1.3
T478K	15.9 ± 1.9	0.9 ± 0.0	−5.1 ± 0.1	−10.5 ± 0.1	−5.4 ± 0.1
L452R/T478K	1,150 ± 100	0.8 ± 0.1	−7.2 ± 0.5	−7.8 ± 0.2	−0.7 ± 0.5

variant with high probability. None of the two mutations L452R and T478K were part of Alpha, Beta, and Gamma VOCs, and only T478K (and not L452R) is present in the recently discovered Omicron VOC. In this manuscript, we examined the effect of these two novel mutations on the biophysical fitness landscape of Delta variant RBD.

Delta VOC displays unique biophysical characteristics unlike the previous VOCs Alpha, Beta, and Gamma. Biophysical data on Omicron VOC is not yet available, and hence we will be comparing the results on Delta VOC with other VOCs discovered prior to Delta. Table 7 lists the summary of biophysical parameters we have examined. Delta mutations do not significantly alter the binding affinity of RBD towards the ACE2 receptor (Figure 4 and Table 1). While a common belief is that VOCs should result in increased binding to ACE2, which would correlate with increased viral entry, data on Delta variant shows that this cannot be a ubiquitous thought. VOC having no effect on ACE2 binding affinity is unique to the Delta variant, as all previous VOCs showed increased affinity to ACE2.[10,34] This is primarily because of the presence of N501Y mutation in previous VOCs that is responsible for increased ACE2 binding.[35,64,65] Delta VOC does not contain N501Y mutation, whereas all other VOCs including Omicron contains the N501Y mutation. In addition, neither L452 nor T478 have a direct interaction with ACE2 (Figure 3(A)). ACE2 binding has been one of the most common factors when attempting to predict emerging VOCs,[12] which would explain why the two novel RBD mutations that resulted in the Delta variant have not been predicted by earlier studies. Thus, it is important to consider a more robust system for predicting variants that is not so

heavily weighted towards ACE2 binding, as our results show that immune escape rather than increased receptor binding compared to the WT RBD determines the fitness of Delta VOC. Since the full-length spike protein exists in multiple conformations with RBDs in up or down positions,[13,66] measured binding affinity for isolated RBD towards ACE2 represents the upper value of the binding affinity. Any conformation with RBD in down position in equilibrium will only decrease the relative population of RBDs in up conformation, and hence will result in decreased affinity of the complete spike protein towards ACE2.

Compared to other VOCs, patients contracted with Delta have increased viral titers.[15,67] Results show that the two Delta mutations did not affect either the secondary (far-UV CD; Figure 2(B)) or tertiary structure (intrinsic protein fluorescence of aromatic sidechains; Figure 2(C)) of the RBD. This is consistent with the three-dimensional structural alignment of the two RBDs using the Multiprot program.[68] Delta RBD (PDB ID: 7v8b) has similar structure as that of WT RBD (PDB ID: 6m0j) with an RMSD of 0.82 Å. Additionally, the two mutations L452R and T478K did not alter the stability of the RBD when measured by both thermal denaturation (Figure S1 and Table S1) or urea denaturation (Figure S2 and Table S2) experiments. However, Delta RBD showed ∼70% higher expression in human Expi293 (modified HEK293) cells compared to the WT RBD (Figure 1). Similar high expression of RBD was not seen in the case of Alpha, Beta, and Gamma VOCs.[10] Increased expression of RBD is determined by the L452R mutation (Figure 1 and Table 7), and this mutation is not present in other VOCs. One single mutation increasing the native protein expression by 70% is very rare in protein lit-

Table 7 Biophysical parameters determining the fitness of SARS-CoV-2 Delta variant RBD. Statistical analyses of mutant properties with respect to the WT were performed using unpaired t-test, and P-values less than 0.05 were considered significant. Superscripts indicate *P < 0.05, **P < 0.01, ***P < 0.001, and no superscript indicates not a significant difference between the mutant and the WT.

RBD variant	Expression	T_m (°C)	$\Delta G°_{unf}$ (kcal/mol)	ACE2 K_d (nM)	Class 1 CC12.1 K_d (nM)	Class 1 LY-CoV016 K_d (nM)	Class 2 P2B-2F6 K_d (nM)	Class 2 LY-CoV555 K_d (nM)	Class 3 REGN10987 K_d (nM)
WT	-	56.1 ± 0.7	8.1 ± 0.3	10.0 ± 3.1	28.0 ± 8.8	49.3 ± 10.1	81.4 ± 6.2	3.9 ± 1.9	34.3 ± 8.1
L452R	**Increase* (+71%)**	56.5 ± 0.2	8.1 ± 0.2	6.2 ± 3.7	13.0 ± 3.4	23.4 ± 2.8	**No binding***	**No binding***	1,340 ± 100***
T478K	No Change (+2%)	54.1 ± 0.1*	7.9 ± 0.5	17.1 ± 4.8	23.1 ± 2.3	15.4 ± 3.0	80.5 ± 0.3	9.0 ± 4.6	15.9 ± 1.9
L452R/T478K	**Increase* (+68%)**	56.6 ± 0.2	6.8 ± 0.2	10.8 ± 3.3	12.4 ± 7.3	10.8 ± 1.4	**No binding***	**No binding***	1,150 ± 100**

erature in general. Increased expression of viral proteins can lead to increased viral titers, although whether L452R results in increased expression of the complete spike protein needs to be examined. If that is the case, relative expression levels of viral protein mutants need to be considered as a criterion in predicting the emergence of future VOCs.

Another crucial factor to consider when evaluating viral fitness is the ability of mutations to escape neutralizing antibodies generated by human immune system in response to WT SARS-CoV-2 infection or vaccination, or those authorized by FDA for treating infected patients. Determining whether the variants escape FDA-approved antibodies, which are derived either from patients recovered from WT SARS-CoV-2 infection (Eli Lilly) or from humanized mice models (Regeneron), will tell us whether the current therapies work against the emerging variants or new antibody therapies need to be developed. Neutralizing antibodies have been broadly classified into different classes depending on the location of their epitopes on RBD.[48,49] Identifying mutations in the structures of RBD-antibody complexes (Figure 3) and analyzing the stabilizing interactions in which they participate can sometimes predict which antibodies the VOCs can escape. However, experiments have to confirm such predictions based on protein structure because long-range mutation effects and the dynamics of various protein regions can play a critical role in protein function. The two mutations L452R and T478K are far away from the binding interface of two Class 1 antibodies we examined (CC12.1 (Figure 3(B)) and FDA-approved Eli Lilly Class 1 antibody LY-CoV016 (Figure 3(C))), and both mutations are not part of the RBD interface with Class 1 antibodies. Consistently, Delta mutants did not escape Class 1 antibodies (Figure 5, Figure 6, Table 2, Table 3 and Table 7). In contrast, L452 stabilizes the RBD interactions with Class 2 antibodies by forming a hydrophobic cluster with I103 and V105 of the variable heavy chain of P2B-2F6 and I54 and L55 residues of the variable heavy chain of LY-CoV555. Replacing the hydrophobic residue leucine with a positively charged arginine in the middle of these hydrophobic clusters is expected to destabilize the RBD interactions with Class 2 antibodies. Accordingly, after L452R mutation, RBD did not bind to Class 2 antibodies (Figure 7, Figure 8, Table 4, Table 5 and Table 7). In the case of RBD binding to Class 3 antibodies (Figure 3(F)), L452 does not form any direct contacts with the antibody REGN10987, but neighbors the epitope composed of residue N450 in RBD.[69,70] Change of a hydrophobic amino acid leucine with a positively charged residue arginine next to the epitope is expected to change the electrostatic nature of RBD interface with REGN10987, and thus might explain the decrease in binding affinity by ~100-fold upon L452R mutation (Figure 9, Table 6 and Table 7).

T478 residue in RBD is far away from any of the binding interfaces with neutralizing antibodies and do not participate in any stabilizing inter-molecular interactions, and hence do not contribute to the immune escape potential of the Delta variant (Table 7).

Our results indicate that L452R mutation determines the antigenic drift of the Delta VOC against Class 2 and Class 3 antibodies. Since L452R also occurs in other variants such as Epsilon, Iota, and Kappa,[71] we expect these variants also escape Class 2 and Class 3 antibodies. Despite the number of infected cases with T478K mutation are increasing,[72,73] its role in the viral fitness is quite elusive. Our results indicate that it does not offer any fitness advantage to SARS-CoV-2 RBD in terms of receptor binding or immune escape from neutralizing antibodies compared to the WT. Some studies have suggested that T478K mutation might have evolved from previously infected Beta VOC patients, since it escapes an antibody specific to the Beta VOC.[74] In addition, the newest Omicron VOC contains S477N mutation in addition to T478K mutation, and whether T478K mutation enhances the antibody escape determined by S477N needs to be examined. Further, our study has examined the role of T478K mutation on the biophysical properties of RBD, and its specific role needs to be examined in the context of the full-length spike protein, particularly in controlling the up/down conformations of the spike protein and long-range allosteric effects on other important structural regions of the spike protein.

Results presented here indicate that the Delta variant has evolved towards escape from Class 2 and Class 3 antibodies, rather than enhancing the receptor binding or escape from Class 1 antibodies. Class 1 antibodies bind to RBD only in up conformation where RBD is accessible to ACE2 binding, whereas Class 2 and Class 3 antibodies bind to RBD irrespective of whether it is in up conformation (accessible to ACE2) or down conformation (inaccessible to ACE2).[49] Escape from Class 2 antibodies mainly contributes to escape from polyclonal plasma,[56] which might be more important for virus survival than escape from Class 1 antibodies that target only a sub-population of the spike protein trimers with their RBDs in up conformation. Further, since Class 2 and Class 3 antibodies can bind to RBD irrespective of whether it is in up (ACE2 accessible) or down (ACE2 inaccessible) conformation, these antibodies can recognize adjacent RBDs in the spike trimer and once bound they can lock RBDs in down conformation thereby restricting binding to ACE2;[75] hence, the virus escaping from Class 2 and Class 3 antibodies might be more relevant for the spike protein of the variants to bind to ACE2 leading to increased infection. In terms of the efficacy of the current FDA-approved antibody therapies, both Eli Lilly's Class 1 antibody LY-CoV016 and Regeneron's Class 1 antibody REGN10933 should be effective in neutralizing the Delta variant, since the Delta mutations did not affect RBD binding to Class 1 antibodies (Table 7). However, Eli Lilly's Class 2 antibody LY-CoV555 will be completely ineffective in neutralizing the Delta variant as L452R completely abolished RBD binding to Class 2 antibodies, whereas Regeneron's Class 3 antibody REGN10987 will be much less effective and requires much higher concentration to neutralize the virus as the RBD binding affinity is reduced by ~100 fold upon Delta mutations (Table 7).

The immune escape and high expression capabilities of the SARS-CoV-2 Delta variant requires a necessity for robust therapeutic options. As the virus adapts, every successive VOC has shown increased immune escape potential. Thus, new vaccines need to be developed and administered based on the variant sequences existing at the time of vaccination, and it is necessary for the vaccination rates to continue to rise in order to combat the emergence of future VOCs. Simultaneously, it is necessary for improved monoclonal antibody therapeutics to be developed against future variants. Delta VOC is clearly distinct from other VOCs. Our previous work has shown that other VOCs can escape Class 1 antibodies, while expression is not significantly different from that of the unmutated WT.[10] Delta does not escape Class 1 antibodies and shows higher protein expression. In addition, all previously studied variants showed enhanced ACE2 binding which is not the case for the Delta variant. These results also point to the fact that the virus is still under continuous evolution, as none of the VOCs is still able to escape all classes of neutralizing antibodies. Any combination of mutations that confer immune escape potential to SARS-CoV-2 against all classes of neutralizing antibodies will be of a major concern. In terms of applicability of our results to the new Omicron variant, Omicron might still show higher ACE2 binding because of the presence of N501Y mutation. Since Omicron lacks L452R mutation, it might not escape Class 2 and Class 3 antibodies, unless a separate set of amino acid mutations confer the ability to escape these neutralizing antibodies. Since Omicron is the most transmissible and Delta is the most virulent out of the five known VOCs, if Omicron picks up the critical Delta mutations resulting in a Deltacron variant, it could turn out to be a more dangerous variant.

Note added during Revision: As predicted above, recent results show that Omicron VOC has higher ACE2 binding.[76] It escapes Class 2 and Class 3 neutralizing antibodies,[74,77] and the escape has to be due to a different set of mutations since initial Omicron variants lacked L452R mutation. Recent Omicron subvariants BA.4 and BA.5 have picked up the L452R mutation that was specific to Delta VOC, and the number of infected cases are increasing again.

Materials and Methods

Cloning

Sequences for RBD and human ACE2 were obtained from Uniprot (RBD ID: P0DTC2; hACE2 ID: Q9BYF1). Sequences for neutralizing antibodies were obtained from Research Collaboratory for Structural Bioinformatics (RCSB) Protein Data Bank (PDB). CC12.1, LY-CoV016, P2B-2F6, LY-CoV555, and REGN 10987 had PDB IDs of 6XC2, 7C01, 7BWJ, 7KMG, and 6XDG respectively. Antibody constructs were designed in ScFv format, linking the heavy chain (V_H) and light chain (V_L) via a glycine serine linker. Final ScFv constructs were $V_H - (GGGGS)_3–V_L$. All sequences were codon optimized for expression in mammalian cells by Twist Biosciences. Final constructs included the protein of interest, SUMOstar protein attached to a His-tag, and a human immunoglobulin heavy chain secretory sequence from 5′ to 3′ position. RBD variants were created by site-directed mutagenesis. Sequences were cloned into a pcDNA3.4-TOPO vector. Expi293 HEK cells were transfected at a concentration of 3×10^6 cells/mL with polyethyleneimine. Proteins were expressed over a 5-day period, and the culture media was centrifuged and the supernatant was filter sterilized with a 0.22 μm PVDF filter. The expression levels for individual mutants were compared after running the culture supernatants on SDS-PAGE, staining with Coomassie blue R-250 dye, and quantifying the band intensities corresponding to the target protein normalized to cell density using the ImageLab software from Bio-Rad.

Purification

All proteins were purified using a Ni-NTA column, and the protein was eluted with 200 mM imidazole. The eluted protein was dialyzed to remove imidazole and stored in a buffer consisting of 50 mM Tris, 200 mM NaCl, pH 8.0. The proteins were cleaved using SUMOstar protease at 4 °C overnight. Proteins were once again passed through a Ni-NTA column, and the digested proteins were collected in the flow-through and wash. Proteins were dialyzed into a buffer solution of 50 mM sodium phosphate, 20 mM NaCl, pH 7.0. Purity was confirmed by SDS-PAGE.

CD spectroscopy

An Applied Photophysics Chirascan Plus spectrometer was used to record the CD spectra and thermal denaturation melts for all variants. CD Spectra were obtained for each RBD variant from 190 nm to 260 nm. Protein spectra were recorded with a 0.5 mm cuvette at 5 μM protein concentration in a buffer consisting of 10 mM sodium phosphate, 4 mM NaCl, pH 7.0. Spectra were recorded every 1 nm wavelength and averaged over 2 seconds. Runs were repeated 5 times and averaged.

Thermal denaturation melts were performed using an Applied Photophysics Chirascan Plus spectrometer. All experiments were performed in a 0.5 mm cuvette at a protein concentration of 20 μM in buffer containing 50 mM sodium phosphate, 20 mM NaCl, pH 7.0. Temperature scan rate was 1 °C/min, sample was equilibrated for 30 sec at each temperature increment, and the CD signal at 222 nm was averaged over 2 seconds. Data was plotted and analyzed using the equation.[47]

$$S_T = \frac{(S_N + m_N T) + (S_U + m_U T)e^{-(\frac{\Delta H_m}{R}(\frac{1}{T} - \frac{1}{T_m}))}}{1 + e^{-(\frac{\Delta H_m}{R}(\frac{1}{T} - \frac{1}{T_m}))}} \quad (1)$$

where S_T is the measured signal as a function of temperature T, S_N and S_U are the signals corresponding to the native and unfolded baselines, m_N and m_U are the slopes of linear dependence of S_N and S_U with temperature, T_m is the midpoint melting temperature, ΔH_m is the enthalpy change at the T_m, R is the universal gas constant, and T is the absolute temperature in Kelvin, respectively.

Fluorescence spectroscopy

A CCD detector was used with the Applied Photophysics Chirascan Plus spectrometer to record the fluorescence spectra and chemical denaturation for all variants. An excitation wavelength of 280 nm was used, and fluorescence emission was recorded in a 1 cm cuvette at 2 μM protein concentration in a buffer containing 50 mM sodium phosphate, 20 mM NaCl, pH 7.0. Urea was utilized as the denaturant for equilibrium protein unfolding measurements, and was dissolved in 50 mM sodium phosphate, 20 mM NaCl, pH 7.0 buffer. The concentration of the urea solution was determined using refractive index measurements.[78,79] Two end solutions were made (protein in buffer with no denaturant and in ∼9 M urea), equilibrated for 1 hour, and were mixed at urea concentration intervals of 0.2 M using a Hamilton dual syringe automated titrator attached to the spectrometer. Samples were equilibrated for 10 min in between titrations, and the change in spectral data was analyzed using the equation.[80]

$$S_D = \frac{(S_N + m_N [D]) + (S_U + m_U [D])e^{-(\Delta G°_{unf} + m[D])/RT}}{1 + e^{-(\Delta G°_{unf} + m[D])/RT}} \quad (2)$$

where S_D is the signal at a denaturant concentration $[D]$, S_N and S_U are the signals corresponding to the native and unfolded proteins without denaturant, m_N and m_U are the slopes of linear dependence of S_N and S_U with $[D]$, $\Delta G°_{unf}$ is the Gibbs free energy change of unfolding, and m is the slope of linear dependence of ΔG_{unf} with $[D]$, R is the universal gas constant, and T is the absolute temperature in Kelvin, respectively.

ITC binding analysis

ITC was performed on the Malvern Microcal PEAQ-ITC. All experiments were performed in a buffer solution of 50 mM sodium phosphate, 20 mM NaCl, pH 7.0 at 20 °C and consisted of eighteen 2 μL injections spaced every 150 seconds. For RBD-ACE2 interactions, ACE2 was used at a concentration of 15 μM in the cell, while RBD and all variants were injected from a stock solution of 150 μM in the syringe. For RBD-CC12.1 ScFv interactions, RBD was used at a concentration of 25 μM while CC12.1 was injected from a stock solution of 250 μM. RBD-LY-CoV016 interactions were studied at a concentration of 30 μM RBD and LY-CoV016 was injected from a stock solution of 250 μM. RBD-LY-CoV555, RBD-P2B-2F6, and RBD-REGN10987 ScFv interactions were studied using a RBD concentration of 30 μM, while LY-CoV555, P2B-2F6, and REGN10987 ScFvs were injected from a syringe stock concentration of 300 μM. All data was collected and analyzed using the Microcal PEAQ-ITC Data Analysis Software. Errors on ΔG and $-T\Delta S$ were calculated using error propagation formulae.[81]

Statistical analyses

In order to determine the significance of differences between the biophysical properties of WT RBD and mutant proteins, an unpaired t-test was used. Statistical analyses were performed using GraphPad Prism (Version 9.3.1).

CRediT authorship contribution statement

Casey Patrick: Conceptualization, Methodology, Validation, Formal analysis, Investigation, Data curation, Writing – original draft, Writing – review & editing, Visualization. **Vaibhav Upadhyay:** Conceptualization, Methodology, Resources, Writing – review & editing, Visualization. **Alexandra Lucas:** Conceptualization, Methodology, Writing – review & editing. **Krishna M.G. Mallela:** Conceptualization, Methodology, Writing – review & editing, Supervision, Project administration, Funding acquisition.

DATA AVAILABILITY

Data will be made available on request.

Acknowledgements

Declaration of interests

The authors declare that they have no known competing financial interests or personal relationships that could have appeared to influence the work reported in this paper.

Appendix A. Supplementary material

Supplementary data to this article can be found online at https://doi.org/10.1016/j.jmb.2022.167622.

References

1. Chan, K.K., Dorosky, D., Sharma, P., Abbasi, S.A., Dye, J. M., Kranz, D.M., Herbert, A.S., Procko, E., (2020). Engineering human ACE2 to optimize binding to the spike protein of SARS coronavirus 2. *Science* **369**, 1261–1265.

2. Dehury, B., Raina, V., Misra, N., Suar, M., (2021). Effect of mutation on structure, function and dynamics of receptor binding domain of human SARS-CoV-2 with host cell receptor ACE2: a molecular dynamics simulations study. *J. Biomol. Struct. Dyn.* **39**, 7231–7245.

3. Hussain, M., Jabeen, N., Raza, F., Shabbir, S., Baig, A.A., Amanullah, A., Aziz, B., (2020). Structural variations in human ACE2 may influence its binding with SARS-CoV-2 spike protein. *J. Med. Virol.* **92**, 1580–1586.

4. Yin, R., Guest, J.D., Taherzadeh, G., Gowthaman, R., Mittra, I., Quackenbush, J., Pierce, B.G., (2021). Structural and energetic profiling of SARS-CoV-2 receptor binding domain antibody recognition and the impact of circulating variants. *PLoS Comput. Biol.* **17**, e1009380

5. Zoufaly, A., Poglitsch, M., Aberle, J.H., Hoepler, W., Seitz, T., Traugott, M., Grieb, A., Pawelka, E., et al., (2020). Human recombinant soluble ACE2 in severe COVID-19. *Lancet Respir. Med.* **8**, 1154–1158.

6. Tian, D., Sun, Y., Zhou, J., Ye, Q., (2021). The global epidemic of SARS-CoV-2 variants and their mutational immune escape. *J. Med. Virol.*. https://doi.org/10.1002/jmv.27376.

7. Wang, L., Wang, L., Zhuang, H., (2020). Profiling and characterization of SARS-CoV-2 mutants' infectivity and antigenicity. *Signal Transduct Target Ther* **5**, 185.

8. Yurkovetskiy, L., Wang, X., Pascal, K.E., Tomkins-Tinch, C., Nyalile, T.P., Wang, Y., Baum, A., Diehl, W.E., et al.,

(2020). Structural and Functional Analysis of the D614G SARS-CoV-2 Spike Protein Variant. *Cell* **183** 739–751.e8.

9. Salleh, M.Z., Derrick, J.P., Deris, Z.Z., (2021). Structural Evaluation of the Spike Glycoprotein Variants on SARS-CoV-2 Transmission and Immune Evasion. *Int. J. Mol. Sci.* **22**, 7425.

10. Upadhyay, V., Lucas, A., Panja, S., Miyauchi, R., Mallela, K.M.G., (2021). Receptor binding, immune escape, and protein stability direct the natural selection of SARS-CoV-2 variants. *J. Biol. Chem.* **297**, 101208

11. Luan, J., Lu, Y., Jin, X., Zhang, L., (2020). Spike protein recognition of mammalian ACE2 predicts the host range and an optimized ACE2 for SARS-CoV-2 infection. *Biochem. Biophys. Res. Commun.* **526**, 165–169.

12. Zahradnik, J., Marciano, S., Shemesh, M., Zoler, E., Harari, D., Chiaravalli, J., Meyer, B., Rudich, Y., et al., (2021). SARS-CoV-2 variant prediction and antiviral drug design are enabled by RBD in vitro evolution. *Nature Microbiol.* **6**, 1188–1198.

13. McCallum, M., Walls, A.C., Sprouse, K.R., Bowen, J.E., Rosen, L.E., Dang, H.V., De Marco, A., Franko, N., et al., (2021). Molecular basis of immune evasion by the Delta and Kappa SARS-CoV-2 variants. *Science* **374**, 1621–1626.

14. Cherian, S., Potdar, V., Jadhav, S., Yadav, P., Gupta, N., Das, M., Rakshit, P., Singh, S., et al., (2021). SARS-CoV-2 Spike Mutations, L452R, T478K, E484Q and P681R, in the Second Wave of COVID-19 in Maharashtra, India. *Microorganisms* **9**, 1542.

15. Mlcochova, P., Kemp, S.A., Dhar, M.S., Papa, G., Meng, B., Ferreira, I., Datir, R., Collier, D.A., et al., (2021). SARS-CoV-2 B.1.617.2 Delta variant replication and immune evasion. *Nature* **599**, 114–119.

16. Planas, D., Veyer, D., Baidaliuk, A., Staropoli, I., Guivel-Benhassine, F., Rajah, M.M., Planchais, C., Porrot, F., et al., (2021). Reduced sensitivity of SARS-CoV-2 variant Delta to antibody neutralization. *Nature* **596**, 276–280.

17. Thangaraj, J.W.V., Yadav, P., Kumar, C.G., Shete, A., Nyayanit, D.A., Rani, D.S., Kumar, A., Kumar, M.S., et al., (2022). Predominance of delta variant among the COVID-19 vaccinated and unvaccinated individuals, India, May 2021. *J. Infect.* **84**, 94–118.

18. Farinholt, T., Doddapaneni, H., Qin, X., Menon, V., Meng, Q., Metcalf, G., Chao, H., Gingras, M.C., et al., (2021). Transmission event of SARS-CoV-2 delta variant reveals multiple vaccine breakthrough infections. *BMC Med.* **19**, 255.

19. Tretyn, A., Szczepanek, J., Skorupa, M., Jarkiewicz-Tretyn, J., Sandomierz, D., Dejewska, J., Ciechanowska, K., Jarkiewicz-Tretyn, A., et al., (2021). Differences in the Concentration of Anti-SARS-CoV-2 IgG Antibodies Post-COVID-19 Recovery or Post-Vaccination. *Cells* **10**, 1952.

20. Lopez Bernal, J., Andrews, N., Gower, C., Gallagher, E., Simmons, R., Thelwall, S., Stowe, J., Tessier, E., et al., (2021). Effectiveness of Covid-19 Vaccines against the B.1.617.2 (Delta) Variant. *N. Engl. J. Med.* **385**, 585–594.

21. Saito, A., Irie, T., Suzuki, R., Maemura, T., Nasser, H., Uriu, K., Kosugi, Y., Shirakawa, K., et al., (2022). Enhanced fusogenicity and pathogenicity of SARS-CoV-2 Delta P681R mutation. *Nature* **602**, 300–306.

22. Liu, C., Ginn, H.M., Dejnirattisai, W., Supasa, P., Wang, B., Tuekprakhon, A., Nutalai, R., Zhou, D., et al., (2021). Reduced neutralization of SARS-CoV-2 B.1.617 by vaccine and convalescent serum. *Cell* **184**, 4220–4236.e13.

23. Kannan, S.R., Spratt, A.N., Cohen, A.R., Naqvi, S.H., Chand, H.S., Quinn, T.P., Lorson, C.L., Byrareddy, S.N., et al., (2021). Evolutionary analysis of the Delta and Delta Plus variants of the SARS-CoV-2 viruses. *J. Autoimmun.* **124**, 102715

24. Li, M., Lou, F., Fan, H., (2021). SARS-CoV-2 Variants of Concern Delta: a great challenge to prevention and control of COVID-19. *Signal. Transduct. Target. Ther.* **6**, 349.

25. He, X., Hong, W., Pan, X., Lu, G., Wei, X., (2021). SARS-CoV-2 Omicron variant: Characteristics and prevention. *MedComm* **2020** (2), 838–845.

26. Tokuriki, N., Oldfield, C.J., Uversky, V.N., Berezovsky, I.N., Tawfik, D.S., (2009). Do viral proteins possess unique biophysical features? *Trends Biochem. Sci.* **34**, 53–59.

27. Rotem, A., Serohijos, A.W.R., Chang, C.B., Wolfe, J.T., Fischer, A.E., Mehoke, T.S., Zhang, H., Tao, Y., et al., (2018). Evolution on the Biophysical Fitness Landscape of an RNA Virus. *Mol. Biol. Evol.* **35**, 2390–2400.

28. Wang, Y., Lei, R., Nourmohammad, A., Wu, N.C., (2021). Antigenic evolution of human influenza H3N2 neuraminidase is constrained by charge balancing. *Elife* **10**, e72516

29. Dolan, P.T., Taguwa, S., Rangel, M.A., Acevedo, A., Hagai, T., Andino, R., Frydman, J., (2021). Principles of dengue virus evolvability derived from genotype-fitness maps in human and mosquito cells. *Elife* **10**, e61921

30. Dai, L., Du, Y., Qi, H., Huber, C.D., Chen, D., Zhang, T.H., Wu, N.C., Wang, E., Lloyd-Smith, J.O., Sun, R., (2021). Quantifying the Evolutionary Constraints and Potential of Hepatitis C Virus NS5A Protein. *mSystems* **6**, e01111–e01120.

31. Madan, B., Zhang, B., Xu, K., Chao, C.W., O'Dell, S., Wolfe, J.R., Chuang, G.Y., Fahad, A.S., et al., (2021). Mutational fitness landscapes reveal genetic and structural improvement pathways for a vaccine-elicited HIV-1 broadly neutralizing antibody. *Proc. Natl. Acad. Sci. U. S. A.* **118**, e2011653118

32. Yuan, M., Huang, D., Lee, C.D., Wu, N.C., Jackson, A.M., Zhu, X., Liu, H., Peng, L., et al., (2021). Structural and functional ramifications of antigenic drift in recent SARS-CoV-2 variants. *Science* **373**, 818–823.

33. Mannar, D., Saville, J.W., Zhu, X., Srivastava, S.S., Berezuk, A.M., Zhou, S., Tuttle, K.S., Kim, A., et al., (2021). Structural analysis of receptor binding domain mutations in SARS-CoV-2 variants of concern that modulate ACE2 and antibody binding. *Cell Rep.* **37**, 110156

34. Barton, M.I., MacGowan, S.A., Kutuzov, M.A., Dushek, O., Barton, G.J., van der Merwe, P.A., (2021). Effects of common mutations in the SARS-CoV-2 Spike RBD and its ligand, the human ACE2 receptor on binding affinity and kinetics. *Elife* **10**, e70658

35. Tian, F., Tong, B., Sun, L., Shi, S., Zheng, B., Wang, Z., Dong, X., Zheng, P., (2021). N501Y mutation of spike protein in SARS-CoV-2 strengthens its binding to receptor ACE2. *Elife* **10**, e69091

36. Bayarri-Olmos, R., Jarlhelt, I., Johnsen, L.B., Hansen, C.B., Helgstrand, C., Rose Bjelke, J., Matthiesen, F., Nielsen, S.D., et al., (2021). Functional Effects of Receptor-Binding Domain Mutations of SARS-CoV-2 B.1.351 and P.1 Variants. *Front. Immunol.* **12**, 757197

37. Bayarri-Olmos, R., Rosbjerg, A., Johnsen, L.B., Helgstrand, C., Bak-Thomsen, T., Garred, P., Skjoedt, M.-O., (2021). The SARS-CoV-2 Y453F mink variant

displays a pronounced increase in ACE-2 affinity but does not challenge antibody neutralization. *J. Biol. Chem.* **296**, 100536

38. Teyssou, E., Delagreverie, H., Visseaux, B., Lambert-Niclot, S., Brichler, S., Ferre, V., Marot, S., Jary, A., et al., (2021). The Delta SARS-CoV-2 variant has a higher viral load than the Beta and the historical variants in nasopharyngeal samples from newly diagnosed COVID-19 patients. *J. Infect.* **83**, e1–e3.

39. Walsh, D., Mohr, I., (2011). Viral subversion of the host protein synthesis machinery. *Nature Rev. Microbiol.* **9**, 860–875.

40. Diao, B., Wang, C., Wang, R., Feng, Z., Zhang, J., Yang, H., Tan, Y., Wang, H., et al., (2021). Human kidney is a target for novel severe acute respiratory syndrome coronavirus 2 infection. *Nature Commun.* **12**, 2506.

41. Jansen, J., Reimer, K.C., Nagai, J.S., Varghese, F.S., Overheul, G.J., de Beer, M., Roverts, R., Daviran, D., et al., (2022). SARS-CoV-2 infects the human kidney and drives fibrosis in kidney organoids. *Cell Stem Cell* **29** 217–231.e8.

42. Helms, L., Marchiano, S., Stanaway, I.B., Hsiang, T.Y., Juliar, B.A., Saini, S., Zhao, Y.T., Khanna, A., et al., (2021). Cross-validation of SARS-CoV-2 responses in kidney organoids and clinical populations. *JCI Insight* **6**, e154882

43. Maffei, M., Montemiglio, L.C., Vitagliano, G., Fedele, L., Sellathurai, S., Bucci, F., Compagnone, M., Chiarini, V., et al., (2021). The Nuts and Bolts of SARS-CoV-2 Spike Receptor-Binding Domain Heterologous Expression. *Biomolecules* **11**, 1812.

44. Ellis, D., Brunette, N., Crawford, K.H.D., Walls, A.C., Pham, M.N., Chen, C., Herpoldt, K.L., Fiala, B., et al., (2021). Stabilization of the SARS-CoV-2 Spike Receptor-Binding Domain Using Deep Mutational Scanning and Structure-Based Design. *Front. Immunol.* **12**, 710263

45. Argentinian AntiCovid, C., (2020). Structural and functional comparison of SARS-CoV-2-spike receptor binding domain produced in Pichia pastoris and mammalian cells. *Sci. Rep.* **10**, 21779.

46. Laha, S., Chakraborty, J., Das, S., Manna, S.K., Biswas, S., Chatterjee, R., (2020). Characterizations of SARS-CoV-2 mutational profile, spike protein stability and viral transmission. *Infect. Genet. Evol.* **85**, 104445

47. Greenfield, N.J., (2006). Using circular dichroism collected as a function of temperature to determine the thermodynamics of protein unfolding and binding interactions. *Nature Protoc.* **1**, 2527–2535.

48. Taylor, P.C., Adams, A.C., Hufford, M.M., de la Torre, I., Winthrop, K., Gottlieb, R.L., (2021). Neutralizing monoclonal antibodies for treatment of COVID-19. *Nature Rev. Immunol.* **21**, 382–393.

49. Barnes, C.O., Jette, C.A., Abernathy, M.E., Dam, K.A., Esswein, S.R., Gristick, H.B., Malyutin, A.G., Sharaf, N.G., et al., (2020). SARS-CoV-2 neutralizing antibody structures inform therapeutic strategies. *Nature* **588**, 682–687.

50. Wrapp, D., Wang, N., Corbett, K.S., Goldsmith, J.A., Hsieh, C.L., Abiona, O., Graham, B.S., McLellan, J.S., (2020). Cryo-EM structure of the 2019-nCoV spike in the prefusion conformation. *Science* **367**, 1260–1263.

51. Ke, Z., Oton, J., Qu, K., Cortese, M., Zila, V., McKeane, L., Nakane, T., Zivanov, J., et al., (2020). Structures and distributions of SARS-CoV-2 spike proteins on intact virions. *Nature* **588**, 498–502.

52. Walls, A.C., Park, Y.J., Tortorici, M.A., Wall, A., McGuire, A.T., Veesler, D., (2020). Structure, Function, and Antigenicity of the SARS-CoV-2 Spike Glycoprotein. *Cell* **181**, 281–292.e6.

53. Rogers, T.F., Zhao, F., Huang, D., Beutler, N., Burns, A., He, W.T., Limbo, O., Smith, C., et al., (2020). Isolation of potent SARS-CoV-2 neutralizing antibodies and protection from disease in a small animal model. *Science* **369**, 956–963.

54. Wang, D., Ge, Y., Zhong, B., Liu, D., (2021). Specific epitopes form extensive hydrogen-bonding networks to ensure efficient antibody binding of SARS-CoV-2: Implications for advanced antibody design. *Comput. Struct. Biotechnol. J.* **19**, 1661–1671.

55. Yuan, M., Liu, H., Wu, N.C., Lee, C.D., Zhu, X., Zhao, F., Huang, D., Yu, W., et al., (2020). Structural basis of a shared antibody response to SARS-CoV-2. *Science* **369**, 1119–1123.

56. Greaney, A.J., Starr, T.N., Barnes, C.O., Weisblum, Y., Schmidt, F., Caskey, M., Gaebler, C., Cho, A., et al., (2021). Mapping mutations to the SARS-CoV-2 RBD that escape binding by different classes of antibodies. *Nature Commun.* **12**, 4196.

57. Martinez, D.R., Schafer, A., Gobeil, S., Li, D., De la Cruz, G., Parks, R., Lu, X., Barr, M., et al., (2021). A broadly cross-reactive antibody neutralizes and protects against sarbecovirus challenge in mice. *Sci. Transl. Med.*, eabj7125.

58. Wang, P., Nair, M.S., Liu, L., Iketani, S., Luo, Y., Guo, Y., Wang, M., Yu, J., et al., (2021). Antibody resistance of SARS-CoV-2 variants B.1.351 and B.1.1.7. *Nature* **593**, 130–135.

59. Gavor, E., Choong, Y.K., Er, S.Y., Sivaraman, H., Sivaraman, J., (2020). Structural Basis of SARS-CoV-2 and SARS-CoV Antibody Interactions. *Trends Immunol.* **41**, 1006–1022.

60. Ju, B., Zhang, Q., Ge, J., Wang, R., Sun, J., Ge, X., Yu, J., Shan, S., et al., (2020). Human neutralizing antibodies elicited by SARS-CoV-2 infection. *Nature* **584**, 115–119.

61. Tsai, K.C., Lee, Y.C., Tseng, T.S., (2021). Comprehensive Deep Mutational Scanning Reveals the Immune-Escaping Hotspots of SARS-CoV-2 Receptor-Binding Domain Targeting Neutralizing Antibodies. *Front. Microbiol.* **12**, 698365

62. Jones, B.E., Brown-Augsburger, P.L., Corbett, K.S., Westendorf, K., Davies, J., Cujec, T.P., Wiethoff, C.M., Blackbourne, J.L., et al., (2021). The neutralizing antibody, LY-CoV555, protects against SARS-CoV-2 infection in nonhuman primates. *Sci. Transl. Med.* **13**, eabf1906.

63. Starr, T.N., Greaney, A.J., Dingens, A.S., Bloom, J.D., (2021). Complete map of SARS-CoV-2 RBD mutations that escape the monoclonal antibody LY-CoV555 and its cocktail with LY-CoV016. *Cell Rep Med* **2**, 100255

64. Ali, F., Kasry, A., Amin, M., (2021). The new SARS-CoV-2 strain shows a stronger binding affinity to ACE2 due to N501Y mutant. *Med. Drug Discovery* **10**, 100086

65. Khan, A., Zia, T., Suleman, M., Khan, T., Ali, S.S., Abbasi, A.A., Mohammad, A., Wei, D.Q., (2021). Higher infectivity of the SARS-CoV-2 new variants is associated with K417N/T, E484K, and N501Y mutants: An insight from structural data. *J. Cell. Physiol.* **236**, 7045–7057.

66. Gobeil, S.M., Janowska, K., McDowell, S., Mansouri, K., Parks, R., Stalls, V., Kopp, M.F., Manne, K., et al., (2021). Effect of natural mutations of SARS-CoV-2 on spike structure, conformation, and antigenicity. *Science* **373**, eabi6226.

67. Li, B., Deng, A., Li, K., Hu, Y., Li, Z., Shi, Y., Xiong, Q., Liu, Z., et al. (2021). Viral infection and transmission in a large, well-traced outbreak caused by the SARS-CoV-2 Delta variant, Nature Commun 13 (2022) 460

68. Micsonai, A., Wien, F., Bulyaki, E., Kun, J., Moussong, E., Lee, Y.H., Goto, Y., Refregiers, M., et al., (2018). BeStSel: a web server for accurate protein secondary structure prediction and fold recognition from the circular dichroism spectra. *Nucleic Acids Res.* **46**, W315–W322.

69. Starr, T.N., Greaney, A.J., Addetia, A., Hannon, W.W., Choudhary, M.C., Dingens, A.S., Li, J.Z., Bloom, J.D., (2021). Prospective mapping of viral mutations that escape antibodies used to treat COVID-19. *Science* **371**, 850–854.

70. Hansen, J., Baum, A., Pascal, K.E., Russo, V., Giordano, S., Wloga, E., Fulton, B.O., Yan, Y., et al., (2020). Studies in humanized mice and convalescent humans yield a SARS-CoV-2 antibody cocktail. *Science* **369**, 1010–1014.

71. Tchesnokova, V., Kulasekara, H., Larson, L., Bowers, V., Rechkina, E., Kisiela, D., Sledneva, Y., Choudhury, D., et al., (2021). Acquisition of the L452R Mutation in the ACE2-Binding Interface of Spike Protein Triggers Recent Massive Expansion of SARS-CoV-2 Variants. *J. Clin. Microbiol.* **59**, e0092121

72. Di Giacomo, S., Mercatelli, D., Rakhimov, A., Giorgi, F.M., (2021). Preliminary report on severe acute respiratory syndrome coronavirus 2 (SARS-CoV-2) Spike mutation T478K. *J. Med. Virol.* **93**, 5638–5643.

73. Jhun, H., Park, H.Y., Hisham, Y., Song, C.S., Kim, S., (2021). SARS-CoV-2 Delta (B.1.617.2) Variant: A Unique T478K Mutation in Receptor Binding Motif (RBM) of Spike Gene. *Immune Netw.* **21**, e32

74. Dejnirattisai, W., Huo, J., Zhou, D., Zahradník, J., Supasa, P., Liu, C., Duyvesteyn, H.M.E., Ginn, H.M., et al., (2022). SARS-CoV-2 Omicron-B.1.1.529 leads to widespread escape from neutralizing antibody responses. *Cell* **185**, 467–484.e15.

75. Wu, N.C., Yuan, M., Liu, H., Lee, C.D., Zhu, X., Bangaru, S., Torres, J.L., Caniels, T.G., et al., (2020). An Alternative Binding Mode of IGHV3-53 Antibodies to the SARS-CoV-2 Receptor Binding Domain. *Cell Rep* **33**, 108274

76. Mannar, D., Saville, J.W., Zhu, X., Srivastava, S.S., Berezuk, A.M., Tuttle, K.S., Marquez, A.C., Sekirov, I., et al., (2022). SARS-CoV-2 Omicron variant: Antibody evasion and cryo-EM structure of spike protein-ACE2 complex. *Science* **375**, 760–764.

77. VanBlargan, L.A., Errico, J.M., Halfmann, P.J., Zost, S.J., Crowe Jr., J.E., Purcell, L.A., Kawaoka, Y., Corti, D., et al., (2022). An infectious SARS-CoV-2 B.1.1.529 Omicron virus escapes neutralization by therapeutic monoclonal antibodies. *Nature Med.*, 1–6.

78. Pace, C.N., (1986). Determination and analysis of urea and guanidine hydrochloride denaturation curves. *Methods Enzymol.* **131**, 266–280.

79. Warren, J.R., Gordon, J.A., (2002). On the Refractive Indices of Aqueous Solutions of Urea. *J. Phys. Chem.* **70**, 297–300.

80. Santoro, M.M., Bolen, D., (1988). Unfolding free energy changes determined by the linear extrapolation method. 1. Unfolding of phenylmethanesulfonyl. alpha.-chymotrypsin using different denaturants. *Biochemistry* **27**, 8063–8068.

81. Bevington, P.R., Robinson, D.K., (2003). Data reduction and error analysis. McGraw Hill, New York.